Characterization of the IL-15 niche in primary and secondary lymphoid organs in vivo

Guangwei Cui[a,b], Takahiro Hara[a], Szandor Simmons[c], Keisuke Wagatsuma[a,b], Akifumi Abe[a,d], Hitoshi Miyachi[e], Satsuki Kitano[e], Masaru Ishii[c,f], Shizue Tani-ichi[a], and Koichi Ikuta[a,1]

[a]Laboratory of Biological Protection, Department of Biological Responses, Institute for Virus Research, Kyoto University, Kyoto 606-8507, Japan; [b]Graduate School of Medicine, Kyoto University, Kyoto 606-8501, Japan; [c]Department of Immunolgy and Cell Biology, Graduate School of Medicine and Laboratory of Cellular Dynamics, World Premier International Research Center, Immunology Frontier Research Center, Osaka University, Suita 565-0871, Japan; [d]Graduate School of Biostudies, Kyoto University, Kyoto 606-8501, Japan; [e]Reproductive Engineering Team, Institute for Virus Research, Kyoto University, Kyoto 606-8507, Japan; and [f]Japan Science and Technology Agency, Core Research for Evolutionary Science and Technology, Tokyo 102-0075, Japan

IL-15 is a cytokine critical for development, maintenance, and response of T cells, natural killer (NK) cells, NK T cells, and dendritic cells. However, the identity and distribution of IL-15–expressing cells in lymphoid organs are not well understood. To address these questions, we established and analyzed IL-15–CFP knock-in mice. We found that IL-15 was highly expressed in thymic medulla, and medullary thymic epithelial cells with high MHC class II expression were the major source of IL-15. In bone marrow, IL-15 was detected primarily in VCAM-1+PDGFRβ+CD31−Sca-1− stromal cells, which corresponded to previously described CXCL12-abundant reticular cells. In lymph nodes, IL-15–expressing cells were mainly distributed in the T-cell zone and medulla. IL-15 was expressed in some fibroblastic reticular cells and gp38−CD31− double-negative stromal cells in the T-cell zone. Blood endothelial cells, including all high endothelial venules, also expressed high IL-15 levels in lymph nodes, whereas lymphatic endothelial cells (LECs) lacked IL-15 expression. In spleen, IL-15 was expressed in VCAM-1+ stromal cells, where its expression increased as mice aged. Finally, IL-15 expression in blood and LECs of peripheral lymphoid organs significantly increased in LPS-induced inflammation. Overall, we have identified and characterized several IL-15–expressing cells in primary and secondary lymphoid organs, providing a unique perspective of IL-15 niche in immune microenvironment. This study also suggests that some stromal cells express IL-7 and IL-15 differentially and suggests a way to functionally classify different stromal cell subsets.

aging | differentiation | homeostasis | thymus

Coordinated cytokine expression by stromal cells in lymphoid organs is essential for immune system development and activity. IL-15 is a cytokine important for differentiation, maintenance, and function of T cells, natural killer (NK) cells, NK T (NKT) cells, and dendritic cells (DCs) (1, 2). The IL-15 receptor (IL-15R) consists of a unique IL-15R α-chain (IL-15Rα), a β-chain (IL-2/IL-15Rβ), and a common cytokine receptor γ-chain (γc). IL-15 may function through transpresentation of an IL-15/IL-15Rα complex to recipient cells expressing IL-2/15Rβ and γc (2, 3). Previous studies in mice lacking IL-15 or IL-15Rα demonstrated that IL-15 plays a critical role in development and homeostasis of naive CD8 T cells, memory T cells, NK cells, NKT cells, and epidermal and intestinal intraepithelial lymphocytes (IELs) (3–5). Nevertheless, the source of IL-15 in different lymphoid organs is largely unknown.

IL-15 mRNA is constitutively expressed in numerous organs such as placenta, skeletal muscle, and kidney (6). Furthermore, the expression of IL-15 is induced in DCs upon LPS or IFN-γ stimulation and is elevated in epithelial cells by infection (7, 8). Transcription factors such as NF-κB and IFN regulatory factor 1 (IRF-1) reportedly function in its expression (9–11). IRF-1–deficient mice show impaired NK cell development as a result of reduced IL-15 expression in bone marrow stromal cells (12). Furthermore, IL-15 expression is regulated at the translational and posttranslational levels (1). Because IL-15 protein is secreted at low levels, it is barely detectable by antibodies, even after stimulation.

To overcome these difficulties, two independent laboratories constructed IL-15 reporter mice by introducing BAC transgenes harboring genes encoding fluorescent reporters controlled by the IL-15 promoter (13, 14). By using these mice, they detected significant fluorescence signals in CD8+ conventional DCs (cDCs) and macrophages, expression augmented by vesicular stomatitis virus stimulation. However, reporter-expressing cells have not been reported in stromal cell populations. Such an inability to detect IL-15–expressing cells could be explained if BAC transgenes lacked regulatory elements required for IL-15 expression in stromal cells. Therefore, the distribution of IL-15–expressing cells is not completely characterized.

Here, to characterize the IL-15–expressing cells in vivo, we established a unique reporter mouse line, in which an enhanced CFP cDNA was inserted into the endogenous IL-15 locus. By using the IL-15–CFP knock-in mice, we revealed IL-15–expressing stromal cells showing a distinct distribution in primary and secondary lymphoid organs. Moreover, we demonstrated age-dependent augmentation and LPS-induced enhancement of IL-15 expression in some stromal cells. Thus, we have identified a unique category of IL-15–expressing cells by using an IL-15-CFP knock-in mouse that serves as a sensitive tool to dissect IL-15 niche in vivo. Taken together with previous observations of IL-7–GFP knock-in mice, we suggest that IL-7 and IL-15 are expressed in the immune microenvironment in distinct but occasionally overlapping patterns.

Results

Generation of IL-15-CFP Knock-in Mice. To determine the distribution of IL-15–producing cells in vivo, we generated IL-15–CFP

Significance

IL-15 is a cytokine critical for development and maintenance of T lymphoid cells. However, the identity and distribution of IL-15–expressing cells in lymphoid organs are not well understood. The present study reveals, by using IL-15–CFP knock-in mice that IL-15 was expressed in subsets of thymic epithelial cells, bone marrow stromal cells, lymph node stromal cells, and blood endothelial cells, a unique perspective of IL-15 niche in immune microenvironment. Taken together with our previous observation on IL-7–producing cells, this study suggests that some stromal cells express IL-7 and IL-15 differentially. Thus, the immune microenvironment appears to be consisted of functionally distinct subsets of stromal cells, expressing different cytokines.

IMMUNOLOGY

knock-in mice. CFP cDNA and a neomycin resistance cassette were inserted at the ATG codon of the third IL-15 exon by homologous recombination (Fig. S1). The neomycin cassette was then removed by Cre recombinase. We analyzed IL-15–CFP heterozygotes in all experiments. IL-15–CFP mice showed normal development of lymphoid organs.

IL-15 Is Highly Expressed in Thymic Medulla. Previous reports demonstrated significantly reduced numbers of thymic NK and NKT cells in IL-15 KO mice, although the source of IL-15 had not been identified (5). To detect an IL-15 signal directly, we performed multiphoton microscopy by using thymus freshly excised from IL-15–CFP mice and littermate controls. CFP signals were clearly detected in thymus, and many were clustered in distinct areas (Fig. S2A).

To identify IL-15–expressing cells in thymus, we performed immunohistochemistry by using an anti-GFP antibody combined with staining of cortical thymic epithelial cells (TECs; cTECs) and medullary TECs (mTECs) with anti-Ly51 and anti-EpCAM antibodies, respectively. Surprisingly, IL-15–expressing cells were predominantly localized in the thymic medulla and displayed EpCAM staining, whereas a few were scattered in corticomedullary junction and coexpressed Ly51 marker (Fig. 1A). Furthermore, many mTECs expressing IL-15 also expressed high levels of MHC class II (MHC-II^{high}) in thymic medulla (Fig. 1B). We also stained blood endothelial cells (BECs) and pericytes with anti-CD31 and anti-PDGFRβ antibodies, respectively, and found that most BECs and some pericytes expressed IL-15, primarily in the thymic medulla (Fig. 1C). To discriminate between hematopoietic and nonhematopoietic cells, we stained DCs and macrophages with anti-CD11c and anti-CD11b antibodies as well as anti-CD31 and anti-GFP antibodies. In contrast to IL-15–expressing CD31$^+$ BECs, DCs, and macrophages in thymus lacked IL-15

Fig. 1. Distribution of IL-15–expressing cells in primary lymphoid organs. Immunohistochemical analysis of thymus (A–C) and bone marrow (D) of 6- to 10-wk-old IL-15–CFP knock-in mice (IL-15$^{CFP/+}$) and control WT littermates. CFP signals were detected with anti-GFP antibody. (A and B) mTECs and cTECs were stained with anti-EpCAM (red) and anti-Ly51 (blue) antibodies, respectively. Most CFP$^+$ cells (green) in medulla display the mTEC marker and these double stained (red and green overlap) cells appear yellow, whereas a few cTECs at the corticomedullary junction also express IL-15 (A, arrowheads). CFP$^+$ mTECs were costained with anti–MHC-II antibody, and these triple-stained cells (red, green, and blue overlap) appear white (B, arrowheads). C, cortex; M, medulla. (C) BECs and pericytes were stained with anti-CD31 (green) and anti-PDGFRβ (light blue) antibodies, respectively. BECs and pericytes (arrows) colocalized with CFP$^+$ cells (red). These double stained cells appear yellow and white, respectively. (D) VCAM-1$^+$ stromal cells (blue), which are primarily adjacent to blood vessels (arrows), express high levels of CFP (red). Data represent three independent experiments with similar results. (Scale bar, 100 μm.)

expression (Fig. S2B). These results suggest that MHC-II^{high} mTECs were the major source of IL-15 in the thymus.

IL-15 Expression in Bone Marrow Stromal Cells. IL-15 transpresentation functions in development and homeostasis of NK, NKT, and memory CD8 T cells in bone marrow (15, 16). To monitor IL-15 signals, we carried out multiphoton microscopy with calvaria of IL-15–CFP mice and littermate controls in vivo. We found that some IL-15–expressing cells were distributed around small blood vessels in bone marrow (Fig. S2C). To further characterize IL-15–expressing cells, we stained cryosections of bone marrow with anti–VCAM-1 (for bone marrow stromal cells) and anti-GFP antibodies. IL-15–expressing cells were scattered throughout the entire bone marrow (Fig. 1D). Most IL-15 signals colocalized with VCAM-1$^+$ stromal cells. Furthermore, numerous VCAM-1$^+$ stromal cells exhibiting an extended triangular morphology and located adjacent to blood vessels expressed high levels of IL-15 (Fig. 1D, Left). We also performed multiphoton microscopy with calvaria of IL-15–CFP/IL-7–GFP double knock-in mice in vivo. We found that most IL-15–expressing cells overlapped with IL-7–expressing cells, whereas some IL-7–expressing cells lacked IL-15 expression in bone marrow (Fig. S2D).

Differential IL-15 Expression in Thymic Stromal Populations. We next characterized the nature of IL-15–expressing cells in thymus by flow cytometry using anti-GFP antibody. We carried out flow cytometry of CD45$^-$Ter119$^-$ thymic stromal cells. TECs were separated into three subsets with anti-Ly51, anti-EpCAM, and anti–MHC-II antibodies (Fig. 2A). MHC-II^{high} mTECs expressed high IL-15 levels, whereas a small fraction of MHC-II^{low} mTECs and cTECs expressed low levels of IL-15 (Fig. 2B). Consistent with data derived from immunohistochemistry and flow cytometry, endogenous IL-15 transcript levels were significantly higher in MHC-II^{high} mTECs than in MHC-II^{low} mTECs and cTECs sorted from WT mice (Fig. 2C). We also separated EpCAM$^-$ nonepithelial stromal cells into CD31$^+$ BECs and EpCAM$^-$CD31$^-$PDGFRβ$^+$ stromal cells, the last of which contained pericytes (Fig. 2D). Approximately 60% to 70% BECs and a subset of EpCAM$^-$CD31$^-$PDGFRβ$^+$ stromal cells expressed IL-15 (Fig. 2E). Overall, these results demonstrate that MHC-II^{high} mTECs are the major source of IL-15, whereas other TECs, BECs, and some pericytes express lower IL-15 levels.

IL-15 Is Highly Expressed in a Fraction of Mesenchymal Stromal Cells in Bone Marrow. The major source of IL-15 in bone marrow is reportedly a distinctive stromal cell population known as CXCL12-abundant reticular (CAR) cells (17). We separated CD45$^-$Ter119$^-$ bone marrow stromal cells into CD31$^+$Sca-1$^+$ BECs, CD31$^-$Sca-1$^+$ cells, and VCAM-1$^+$PDGFRβ^{low}CD31$^-$Sca-1$^-$ and VCAM-1$^+$PDGFRβ^{high}CD31$^-$Sca-1$^-$ stromal cells (Fig. 2F), and assessed CFP expression. More than 60% of VCAM-1$^+$PDGFRβ^{high}CD31$^-$Sca-1$^-$ CAR cells expressed high IL-15 levels, whereas a subset of CAR cells lacked IL-15 expression. In addition, fewer than 10% of VCAM-1$^+$PDGFRβ^{low}CD31$^-$Sca-1$^-$ stromal cells expressed low levels of IL-15, and BECs and CD31$^-$Sca-1$^+$ stromal cells in bone marrow completely lacked IL-15 expression (Fig. 2G). IL-15 and CXCL12 transcripts were analyzed in BECs and in CFP$^+$ and CFP$^-$ CAR cells sorted from IL-15–CFP mice using quantitative RT-PCR. IL-15 transcript levels were significantly greater in the CFP$^+$ fraction of CAR cells than in CFP$^-$ CAR cells and BECs (Fig. 2H). Strikingly, CXCL12 transcripts were highly expressed in CFP$^+$ and CFP$^-$ CAR cells compared with BECs (Fig. 2I). These results indicate that IL-15 is expressed primarily in a subset of CAR cells.

IL-15 Is Expressed in the T-Cell Zone and Medulla of Lymph Nodes. Apart from its role in primary lymphoid organs, IL-15 is also critical for homeostasis of T, NK, and NKT cells in the periphery (4, 5). Thus, we examined peripheral lymph nodes by immunohistochemistry with anti-gp38 [for fibroblastic reticular cells (FRCs)], anti-CD11c
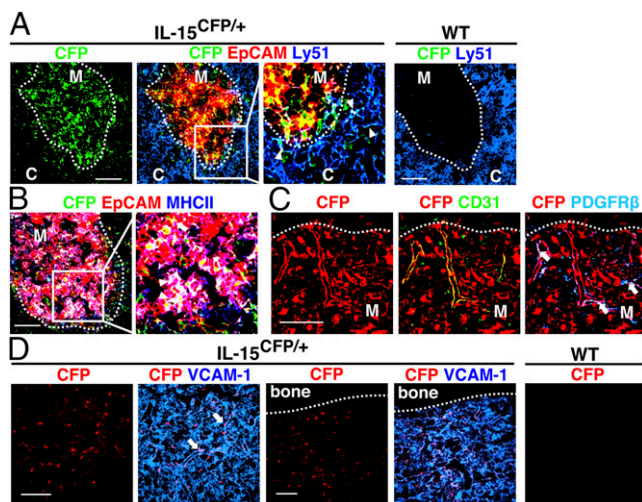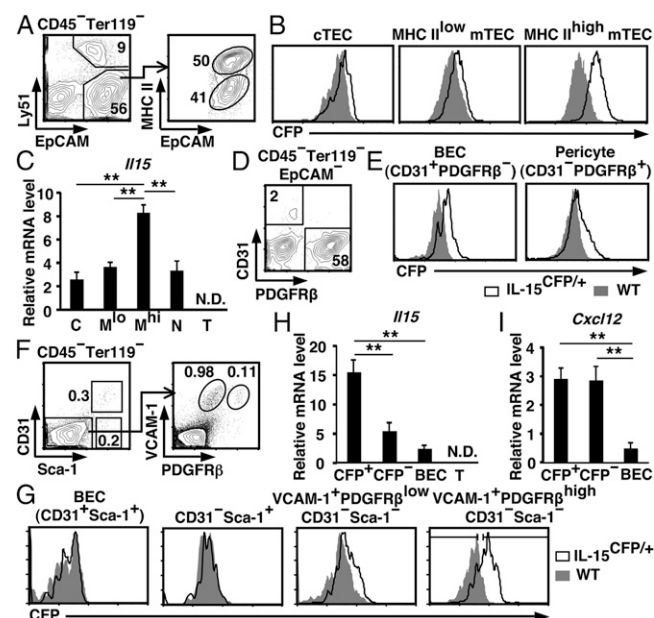
Fig. 2. Characterization of IL-15–expressing cells in thymus and bone marrow. Flow cytometric analysis of IL-15–expressing cells in thymus (*A*, *B*, *D*, and *E*) and bone marrow (*F* and *G*). Stromal cells were isolated from 6- to 10-wk-old IL-15–CFP knock-in mice (IL-15$^{CFP/+}$) and control WT littermates. CFP signals were detected by cytoplasmic staining with anti-GFP antibody. (*A* and *B*) Isolation and CFP expression of TEC subsets. (*C*) IL-15 mRNA levels were measured by real-time RT-PCR in TEC subsets isolated as shown in *A*: cTECs (marked as "C"), MHC-II^{low} mTECs (M^{lo}), MHC-II^{high} mTECs (M^{hi}), and EpCAM$^-$ non-TECs (marked as "N"). T-cells (marked as "T") from IL-15–CFP knock-in mice served as a negative control. Values are the mean ± SEM of duplicate data points. Data represent three independent experiments with similar results. **$P < 0.01$. ND, not detected. (*D* and *E*) Isolation and CFP expression of thymic stromal cells. (*F* and *G*) Isolation and CFP expression of bone marrow stromal cells. (*H* and *I*) IL-15 and CXCL12 mRNA levels were measured by real-time RT-PCR in bone marrow stromal cells isolated as shown in *G*. CFP$^+$ and CFP$^-$ fractions of VCAM-1$^+$ PDGFRβ^{high}CD31$^-$Sca-1$^-$ stromal cells (CFP$^+$ and CFP$^-$, respectively). Values are the mean ± SEM of duplicate data points. Data represent three independent experiments with similar results. **$P < 0.01$. ND, not detected.

(for DCs), and anti-CD3 (for T cells) antibodies, as well as using an anti-GFP antibody. Interestingly, IL-15–expressing cells were predominant in the T-cell zone and medulla but absent from B-cell–rich follicles in axillary, cervical, and inguinal lymph nodes (Fig. 3 *A* and *B*). In contrast, only a few IL-15–expressing cells were present in the T-cell zone of mesenteric lymph nodes (Fig. 3*B*).

As stromal cells of the lymph node can be divided into four fractions with anti-gp38 and anti-CD31 antibodies (18, 19), we carried out flow cytometry of CD45$^-$Ter119$^-$ lymph node stromal cells and divided them into gp38$^+$CD31$^-$ FRCs, gp38$^+$CD31$^+$ lymphatic endothelial cells (LECs), gp38$^-$CD31$^+$ BECs, and double-negative stromal cells (DNSCs) (Fig. 3*C*). IL-15 was expressed in 40–50% of FRCs but completely absent from LECs. Importantly, more than 80% of BECs expressed significantly high levels of IL-15 in peripheral lymph nodes (Fig. 3*D*, *Upper*). In contrast, whereas BECs expressed high levels of IL-15, only a limited number of FRCs expressed very low levels of IL-15 in mesenteric lymph nodes (Fig. 3*D*, *Lower*). Moreover, some DNSCs in the T-cell zone expressed IL-15 in peripheral lymph nodes (Fig. 3*D*, *Upper*).

We next performed immunohistochemistry with sections of lymph node tissue by using anti-gp38 and anti-CD31 antibodies. Consistent with the flow cytometry results, BECs and FRCs but not LECs expressed IL-15 in lymph nodes (Fig. 3*E*). All high endothelial venules (HEVs) also expressed high IL-15 levels, whereas only approximately half of non-HEV BECs expressed IL-15 (Fig. 3*F*). Some DNSCs in T-cell zones expressed high

IL-15 levels (Fig. 3*G*). We also confirmed IL-15 expression in some hematopoietic subsets such as DCs and macrophages by staining with anti-CD31 and anti-CD11c or anti-CD11b antibodies as well as anti-GFP antibody. We found that some DCs and macrophages adjacent to IL-15–expressing stromal cells were CFP$^+$ in lymph nodes (Fig. S3 *A* and *B*). Additionally, the frequency of DCs and macrophages in all IL-15–expressing cells in T-cell zone was less than 10%. Overall, these results demonstrate that a variety of stromal cells in the T-cell zone and medulla express IL-15 in lymph nodes and that all HEVs show significant IL-15 expression.

Age-Dependent IL-15 Expression in Splenic Stromal Cells. To investigate IL-15–expressing cells in spleen, we analyzed sections of spleen tissue using anti–VCAM-1 (for splenic stromal cells) and anti-CD3 antibodies as well as anti-GFP antibody. CFP signals were very weak in young (1 mo old) mice but nonetheless detectable in VCAM-1$^+$ stromal cells within the T-cell zone and red pulp (Fig. 4*A*). Consistent with previous reports that IL-15 is expressed by DCs in spleen, we found that CD8$^+$ cDCs were the major source of IL-15 in the DC fraction, whereas plasmacytoid DCs completely lacked IL-15 expression (Fig. S3 *C* and *D*).

Because the number of NKT and CD8 T cells increases as mice age (20–22), we asked whether IL-15 expression in spleen also changes with aging. We found that IL-15 expression increased in aging (10 mo old) mice compared with young mice (Fig. 4*A*). To characterize IL-15–expressing cells in aging spleen, we carried
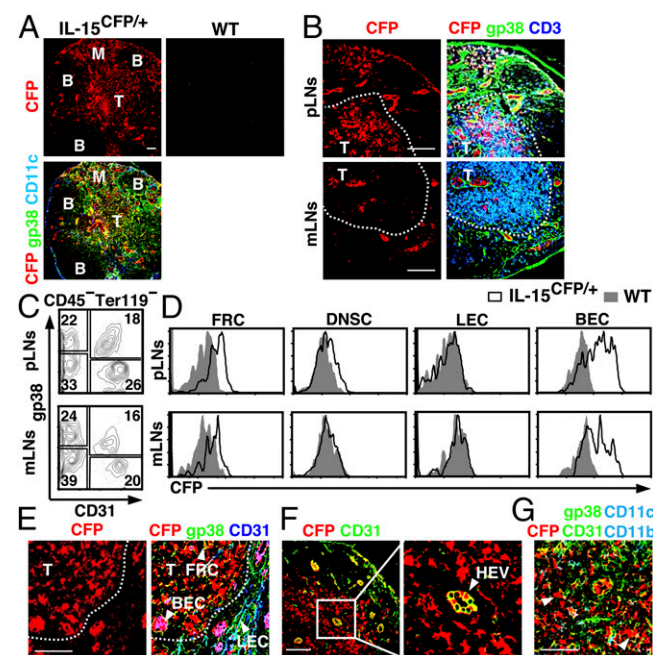

Fig. 3. Characterization of IL-15–expressing cells in lymph nodes. CFP expression in lymph nodes of 8- to 10-wk-old IL-15–CFP knock-in mice (IL-15$^{CFP/+}$) and control WT littermates. CFP signals were detected with an anti-GFP antibody. (*A* and *B*) CFP$^+$ cells in axillary or inguinal lymph nodes (pLN; *A* and *B*, *Upper*) and mesenteric lymph nodes (mLN; *B*, *Lower*). B, B-cell zone; M, medulla; T, T-cell zone. (*C* and *D*) Isolation and CFP expression of lymph node stromal cell fractions. CD45$^-$Ter119$^-$ stromal cells were isolated from axillary, cervical, or inguinal lymph nodes (pLN; *Upper*) and mesenteric lymph nodes (mLN; *Lower*) and divided into FRC (gp38$^+$CD31$^-$), DNSC (gp38$^-$CD31$^-$), LEC (gp38$^+$CD31$^+$), and BEC (gp38$^-$CD31$^+$) fractions with anti-gp38 and anti-CD31 antibodies. (*E*) CFP expression in stromal cells of the T-cell zone. CFP$^+$ FRCs (red and green overlap) and BECs (red and blue overlap) appear yellow and magenta, respectively. LECs (green and blue overlap) appear turquoise. (*F*) CFP expression in CD31$^+$ BECs, including HEVs. CFP$^+$ BECs (red and green overlap) appear yellow. (*G*) CFP expression in some DNSCs (arrowheads, red). Data represent three independent experiments with similar results. (Scale bar, 100 µm.)

out flow cytometry of CD45⁻Ter119⁻ spleen stromal cells with anti–VCAM-1 and anti-CD31 antibodies (Fig. 4B). We observed IL-15 expression in VCAM-1⁺CD31⁻ stromal cells, and the number of CFP⁺ stromal cells as well as CFP levels increased with age, whereas BECs did not express IL-15 at any time point (Fig. 4 C and D). In contrast, IL-15 expression remained unchanged in stromal cell populations of aging lymph nodes (Fig. S4). These results suggest that IL-15 expression in splenic stromal cells is up-regulated in an age-dependent manner.

Endothelial Cells in the Lamina Propria of the Small Intestine Strongly Express IL-15. Several studies indicate that IL-15 produced by intestinal epithelial cells (IECs) supports maintenance of IELs in the small intestine (3, 23). Therefore, we analyzed small intestine tissue sections by immunohistochemistry with anti-EpCAM and anti-CD31 antibodies. Although detection of IL-15 mRNA in IECs has been reported, we observed extremely weak CFP signals only in a few epithelial cells. In contrast, we found some CFP⁺ cells in lamina propria, and many were costained with anti-CD31 antibody (Fig. 4E). Thus, endothelial cells in the lamina propria may express higher IL-15 than IECs in small intestine.

IL-15 Expression Increases Following LPS-induced Inflammation. IL-15 plays a regulatory role in DCs in inflammation induced by LPS

Fig. 4. Characterization of IL-15–expressing cells in spleen and small intestine. CFP expression in spleen and small intestine of IL-15–CFP knock-in mice (IL-15^CFP/+) and control WT littermates. CFP signals were detected with an anti-CFP antibody. (A) CFP⁺ cells in spleen. Stromal cells and T cells were stained with anti–VCAM-1 and anti-CD3 antibodies, respectively. CFP⁺ stromal cells (red and green overlap) appear yellow. (B and C) Age-dependent IL-15 expression in splenic stromal cells. Spleen cells from IL-15–CFP knock-in mice and control WT littermates were stained with anti-CD45, anti–VCAM-1, and anti-CD31 antibodies. BEC represents CD31⁺VCAM-1^low cells. (D) Percentages of CFP⁺ cells in stromal cells and BECs of IL-15–CFP knock-in spleen. Values are the mean ± SEM from three independent experiments. **P < 0.01. (E) IECs and BECs were stained with anti-EpCAM and anti-CD31 antibodies. CFP⁺ IECs (red and green overlap) and BECs (red and blue overlap) appear yellow and magenta, respectively. BECs express high levels of IL-15 (arrowheads), whereas IECs express low levels of IL-15. P, Peyer patch; V, villi. (Scale bar, 100 μm.)

stimulation (7, 24). Thus, we analyzed IL-15 expression in DCs after LPS stimulation. IL-15 expression was slightly up-regulated in cDCs after stimulation (Fig. S5). To analyze IL-15–expressing stromal cells under inflammatory conditions, we injected IL-15–CFP knock-in mice with LPS and assessed potential changes in IL-15 expression 3 d later. In lymph nodes, the number of IL-15–expressing cells significantly increased (Fig. 5A). Surprisingly, induction of IL-15 expression was seen in gp38⁺CD31⁺ LECs after LPS stimulation (Fig. 5A). Furthermore, we gated out hematopoietic cells with anti-CD45, anti-CD11c, and anti-CD11b antibodies by flow cytometry (Fig. S6), and evaluated the alteration of IL-15 expression in stromal cell subsets. In lymph nodes, the level of IL-15 expression by BECs significantly increased, and the proportion of IL-15^high BECs also increased by twofold. IL-15 expression in FRCs and DNSCs was unchanged after LPS administration (Fig. 5 B and C). In spleen, VCAM-1⁺CD31⁻ stromal cells expressed slightly higher IL-15 after stimulation. Notably, IL-15 was slightly induced in BECs by LPS stimulation (Fig. 5 D and E). Overall, these results demonstrate that IL-15 expression in BECs and LECs of peripheral lymphoid organs significantly increases in the presence of LPS-induced inflammation.

IL-15 Expression in Other Organs. As IL-15 mRNA was detected in various organs such as lung, liver, kidney, heart, and skeletal muscle (1, 6), we performed immunohistochemistry of these organs in IL-15–CFP knock-in mice. We did not detect CFP signals in lung, liver, kidney, and skeletal muscle at steady state. However, we found that endocardium of heart expressed IL-15 (Fig. S7A). Furthermore, we observed that liver macrophages expressed high levels of IL-15 after LPS stimulation (Fig. S7 B and C).

Discussion

The cytokine IL-15 plays critical roles in development, maintenance, and response of naive CD8 T cells, memory T cells, NK cells, NKT cells, and IELs. Although IL-15 expression by DCs has been reported, the distribution of IL-15–expressing cells in the stromal cell fraction remains relatively uncharacterized in part because of low protein expression. Recently, others constructed two BAC transgenic mouse lines to track IL-15–expressing cells (13, 14). However, in those mice, detection of IL-15–expressing cells was limited to hematopoietic subsets, possibly because the BAC constructs lack regulatory elements necessary for stromal cell IL-15 expression. We constructed an IL-15–CFP knock-in mouse and observed a variety of IL-15–expressing stromal cells in lymphoid organs, suggesting that IL-15 expression is regulated differently between lymphoid and stromal cells.

MHC-II^high mTECs may be the site for expansion of CD8 T cells and NKT cells in the thymus. IL-7 and other γc cytokines reportedly play a role in their expansion (25, 26). We found that MHC-II^high mTECs produce high levels of IL-15. As IL-15 is a key regulator of development and homeostasis of CD8 T and NKT cells in thymus, the difference in IL-15 expression we observed between medulla and cortex suggests that a distinct IL-15 niche for CD8 T and NKT cells exists in thymic medulla. In that tissue, MHC-II^high mTECs may provide a site for negative selection and maintenance of CD8 T and NKT cells.

CAR cells are the major source of IL-15 in bone marrow. We observed IL-15–expressing cells scattered in the entire bone marrow, many of them VCAM-1⁺PDGFRβ⁺CD31⁻Sca-1⁻ CAR cells. These results are consistent with a report that CAR cells express high levels of IL-15 mRNA (27) and suggest that IL-15–expressing cells support development and homeostasis of memory T, NK, and NKT cells. Interestingly, we identified IL-15⁺ and IL-15⁻ subsets of CAR cells.

IL-15 is critical for proliferation and maintenance of memory T cells, NK cells, NKT cells, and IELs. In lymph nodes, IL-15–expressing cells were localized in the T-cell zone and medulla. We found that some FRCs and DNSCs express IL-15. These stromal cells may function in homeostasis of memory T and NKT
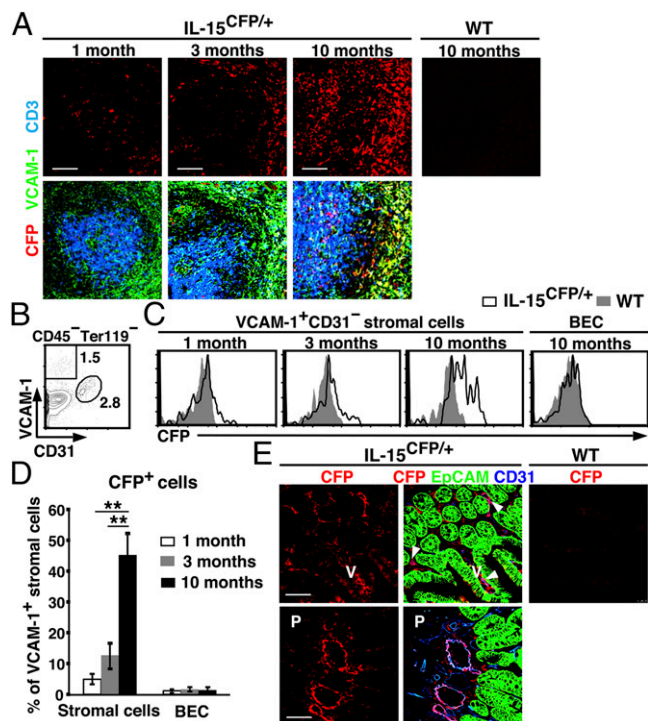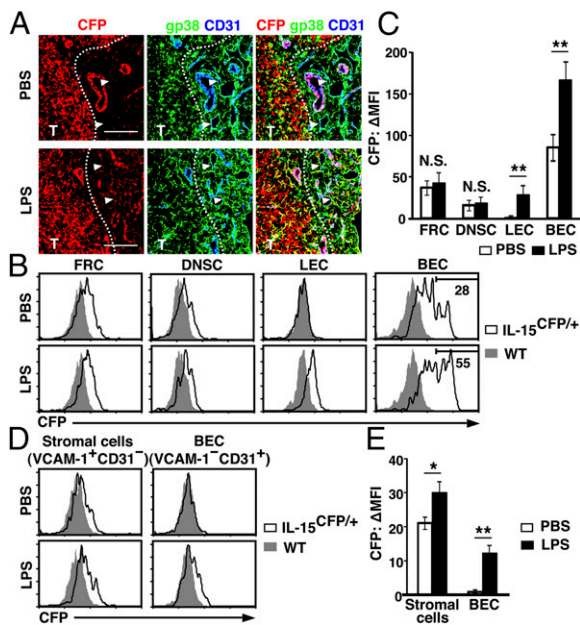
Fig. 5. LPS stimulation induces IL-15 expression in BECs and LECs of peripheral lymphoid organs. Ten-week-old IL-15–CFP knock-in mice (IL-15$^{CFP/+}$) and control WT littermates were injected with LPS. CFP signals were detected with an anti-GFP antibody. (A) Immunohistochemical analysis of lymph nodes 3 d after injection of PBS solution (control; Upper) or LPS (Lower). FRCs and LECs (arrowheads) were stained with anti-gp38 and anti-CD31 antibodies, respectively. CFP$^+$ FRCs (red and green overlap) and BECs (red and blue overlap) appear yellow and magenta, respectively. CFP$^+$ and CFP$^-$ LECs appear white and turquoise, respectively. T, T-cell zone. (Scale bar, 40 μm.) (B) Flow cytometric analysis of lymph nodes 3 d after injection of PBS solution (control; Upper) or LPS (Lower). Hematopoietic cells were gated out with anti-CD45, anti-CD11c, and anti-CD11b antibodies. The percentages of CFP^{high} BECs are shown. (C) The difference in mean fluorescence intensity (ΔMFI) values of CFP between LPS-stimulated and nonstimulated mice, as shown in B. Values are the mean ± SEM from three independent experiments. **P < 0.01. NS, not significant. (D) Flow cytometric analysis of spleen 3 d after injection of PBS solution (control; Upper) or LPS (Lower). (E) The difference in mean fluorescence intensity (ΔMFI) values of CFP between LPS-stimulated and nonstimulated mice as shown in D. Values are the mean ± SEM from three independent experiments. *P < 0.05; **P < 0.01.

cells. One question to be addressed in future studies is whether IL-15–expressing FRCs and DNSCs have equivalent functions.

In spleen, we identified IL-15–expressing VCAM-1$^+$CD31$^-$ stromal cells in the T-cell zone and red pulp. Interestingly, IL-15 expression by splenic stromal cells increased with age. The numbers of memory phenotype CD8 T and NKT cells reportedly increase in the aging spleen (20, 21). Therefore, IL-15–expressing stromal cells may serve as a splenic microenvironment supporting expansion of memory CD8 T and NKT cells.

BECs express IL-15 at high levels. We showed that BECs in thymus, lymph nodes, and Peyer patches express IL-15 at high levels. Remarkably, HEVs in lymph nodes express high IL-15 levels. IL-15 is reportedly important for interaction of T cells with BECs in vitro (28, 29). Our results suggest that IL-15 produced by BECs may function in adhesion and migration of lymphocytes in lymphoid organs.

Inflammation induces IL-15 in multiple cell types. LPS and inflammatory cytokines induce IL-15 in DCs (7). In this study, we showed that LPS also induces IL-15 expression in the stromal cell fraction. LPS-induced inflammation greatly increased IL-15 expression in BECs and LECs, whereas expression in other stromal cells was only slightly increased or unchanged. These results are consistent with reports that TLR4 is expressed in BECs and LECs (30, 31). IL-15 reportedly induces hyaluronate, which

functions in lymphocyte rolling in blood vessels (28). Thus, autocrine secretion of IL-15 by BECs might induce hyaluronate and enhance extravasation of T cells and DCs in inflammation. Moreover, because DCs express IL-15Rα and help lymphocytes enter into lymph nodes through HEVs (32, 33), IL-15 produced by BECs and LECs might activate DCs in inflammation. Thus, IL-15 induction by BECs and LECs may alter lymphocyte migration in inflammation.

IL-7 and IL-15 are differentially expressed in some lymphoid organs (Table S1). We previously reported the distribution of IL-7–producing cells by using IL-7–GFP knock-in mice (34). In thymus, IL-15 is highly expressed in MHC-II^{hi} mTECs, whereas IL-7 is broadly expressed in cTECs and mTECs. Additionally, BECs in thymus expressed IL-15 but not IL-7. In bone marrow, IL-15 and IL-7 are expressed by VCAM-1$^+$CD31$^-$ stromal cells, and especially IL-15 is mainly expressed in a subset of VCAM-1$^+$ PDGFRβ$^+$CD31$^-$Sca-1$^-$ CAR cells. However, IL-15 is not expressed in VCAM-1$^+$CD31$^+$ stromal cells and PDGFRα$^+$Sca-1$^+$ stromal cells, including mesenchymal stem cells and endosteal cells (35, 36), which express high levels of IL-7. Because most IL-15–expressing cells were contained in IL-7–expressing cell population in bone marrow of IL-15–CFP/IL-7–GFP double knock-in mice, some CAR cells seem to express IL-7. IL-15 is expressed in BECs, whereas IL-7 is expressed in LECs of lymph nodes and the intestinal lamina propria. Although FRCs express both IL-7 and IL-15 in lymph nodes, it is not clear whether IL-7- and IL-15–producing cells overlap or constitute different populations because of undetectable levels of direct CFP and GFP fluorescence in secondary lymphoid organs of IL-15–CFP/IL-7–GFP double knock-in mice. Differential expression of IL-7 and IL-15 suggests that the immune microenvironment is organized, at least in part, as a mosaic of different cytokine-producing stromal populations, an arrangement that may facilitate efficient maintenance and responsiveness of lymphoid cells.

In conclusion, we successfully identified and characterized IL-15–expressing cells in primary and secondary lymphoid organs by using IL-15–CFP knock-in mice. Our study provides a perspective of the IL-15 niche in the immune microenvironment and will encourage analysis of the local functions of IL-15 produced by stromal cells in various lymphoid organs. Our study also indicates that IL-7 and IL-15 are differentially expressed by stromal cells and suggests a classification of functionally different stromal cell subsets.

Materials and Methods

Isolation of Stromal Cells. Tissues were dissected into small pieces and incubated in 1 mL of RPMI medium 1640 mixture containing 1.25 mg/mL collagenase D (Roche), 0.8 mg/mL Dispase (Roche), and 0.1 mg/mL DNase (Roche) at 37 °C for 45 min with constant shaking. In the case of lymph nodes and spleen, the mixture also contained 0.2 mg/mL collagenase P (Roche). The cell suspension was gently passed twice through a 24-gauge needle and washed with PBS solution containing 0.5% BSA and 2 mM EDTA (i.e., MACS buffer). Hematopoietic cells were depleted with anti-CD45 and anti-Ter119 microbeads and an LD column (Miltenyi Biotec).

Flow Cytometry. Cells were stained with fluorescent dye- or biotin-conjugated antibodies described in SI Materials and Methods. Hematopoietic cells were gated out with anti-CD45 and Ter119 antibodies. Intracellular staining was performed using FIX & PERM Cell Fixation and Permeabilization reagents (Invitrogen). An anti-GFP antibody (Invitrogen) with cross-reactivity to CFP was used to detect CFP. Stained cells were acquired with a FACS Canto II flow cytometer (BD Biosciences) and analyzed by using FlowJo software (TreeStar). Cell sorting was performed by using a FACSAria II cell sorter (BD Biosciences).

Immunohistochemistry. Tissue sections were prepared and analyzed as described previously (34). After blocking, samples were incubated with the fluorescent dye- or biotin-conjugated antibodies described in *SI Materials and Methods* and then mounted with PermaFluor (Shandon). Bone marrow sections were prepared using the film method (37). Confocal microscopy was performed with TSC-SP5 and TSC-SP8 microscopes (Leica Microsystems).

Real-Time RT-PCR. Total RNA was extracted from sorted cells using Sepasol reagent (Nacalai) and from fixed samples using an RNeasy FFPE kit (Qiagen). cDNA was synthesized with random primers and amplified in duplicate by QuantiTect SYBR Green PCR kit (Qiagen) with ROX (Invitrogen) using an ABI 7500 sequence detector (Applied Biosystems). PCR efficiency was normalized using cDNA of whole thymus or bone marrow from WT mice. Primer sequences were as follows: IL-15 forward, 5′-GTGACTTTCATCCCAGTTGC-3′ and 5′-TTCC-TTGCAGCCAGATTCTG-3′; CXCL12, 5′-GAGCCAACGTCAAGCATCTG-3′ and 5′-CGGGTCAATGCACACTTGTC-3′.

LPS Treatment In Vivo. Mice were injected i.v. with 30 μg of LPS from *Escherichia coli* (Sigma) in 200 μL PBS solution 3 d before the analysis as described previously (7, 38).

Statistics. An unpaired two-tailed Student *t* test was used for all statistical analysis.

1. Waldmann TA, Tagaya Y (1999) The multifaceted regulation of interleukin-15 expression and the role of this cytokine in NK cell differentiation and host response to intracellular pathogens. *Annu Rev Immunol* 17:19–49.
2. Ma A, Koka R, Burkett P (2006) Diverse functions of IL-2, IL-15, and IL-7 in lymphoid homeostasis. *Annu Rev Immunol* 24:657–679.
3. Ma LJ, Acero LF, Zal T, Schluns KS (2009) Trans-presentation of IL-15 by intestinal epithelial cells drives development of CD8αα IELs. *J Immunol* 183(2):1044–1054.
4. Lodolce JP, et al. (1998) IL-15 receptor maintains lymphoid homeostasis by supporting lymphocyte homing and proliferation. *Immunity* 9(5):669–676.
5. Kennedy MK, et al. (2000) Reversible defects in natural killer and memory CD8 T cell lineages in interleukin 15-deficient mice. *J Exp Med* 191(5):771–780.
6. Grabstein KH, et al. (1994) Cloning of a T cell growth factor that interacts with the β chain of the interleukin-2 receptor. *Science* 264(5161):965–968.
7. Mattei F, Schiavoni G, Belardelli F, Tough DF (2001) IL-15 is expressed by dendritic cells in response to type I IFN, double-stranded RNA, or lipopolysaccharide and promotes dendritic cell activation. *J Immunol* 167(3):1179–1187.
8. Zdrenghea MT, et al. (2012) RSV infection modulates IL-15 production and MICA levels in respiratory epithelial cells. *Eur Respir J* 39(3):712–720.
9. Washizu J, Nishimura H, Nakamura N, Nimura Y, Yoshikai Y (1998) The NF-κB binding site is essential for transcriptional activation of the IL-15 gene. *Immunogenetics* 48(1):1–7.
10. Azimi N, Shiramizu KM, Tagaya Y, Mariner J, Waldmann TA (2000) Viral activation of interleukin-15 (IL-15): Characterization of a virus-inducible element in the IL-15 promoter region. *J Virol* 74(16):7338–7348.
11. Azimi N, et al. (1998) Human T cell lymphotropic virus type I Tax protein trans-activates interleukin 15 gene transcription through an NF-κB site. *Proc Natl Acad Sci USA* 95(5):2452–2457.
12. Ogasawara K, et al. (1998) Requirement for IRF-1 in the microenvironment supporting development of natural killer cells. *Nature* 391(6668):700–703.
13. Colpitts SL, et al. (2012) Cutting edge: The role of IFN-α receptor and MyD88 signaling in induction of IL-15 expression in vivo. *J Immunol* 188(6):2483–2487.
14. Sosinowski T, et al. (2013) CD8α+ dendritic cell trans presentation of IL-15 to naive CD8+ T cells produces antigen-inexperienced T cells in the periphery with memory phenotype and function. *J Immunol* 190(5):1936–1947.
15. Schluns KS, et al. (2004) Distinct cell types control lymphoid subset development by means of IL-15 and IL-15 receptor α expression. *Proc Natl Acad Sci USA* 101(15):5616–5621.
16. Becker TC, Coley SM, Wherry EJ, Ahmed R (2005) Bone marrow is a preferred site for homeostatic proliferation of memory CD8 T cells. *J Immunol* 174(3):1269–1273.
17. Sugiyama T, Kohara H, Noda M, Nagasawa T (2006) Maintenance of the hematopoietic stem cell pool by CXCL12-CXCR4 chemokine signaling in bone marrow stromal cell niches. *Immunity* 25(6):977–988.
18. Link A, et al. (2007) Fibroblastic reticular cells in lymph nodes regulate the homeostasis of naive T cells. *Nat Immunol* 8(11):1255–1265.
19. Fletcher AL, et al. (2010) Lymph node fibroblastic reticular cells directly present peripheral tissue antigen under steady-state and inflammatory conditions. *J Exp Med* 207(4):689–697.
20. Pinchuk LM, Filipov NM (2008) Differential effects of age on circulating and splenic leukocyte populations in C57BL/6 and BALB/c male mice. *Immun Ageing* 5:1.
21. Faunce DE, Palmer JL, Paskowicz KK, Witte PL, Kovacs EJ (2005) CD1d-restricted NKT cells contribute to the age-associated decline of T cell immunity. *J Immunol* 175(5):3102–3109.
22. Linton PJ, Dorshkind K (2004) Age-related changes in lymphocyte development and function. *Nat Immunol* 5(2):133–139.
23. Ebert EC (1998) Interleukin 15 is a potent stimulant of intraepithelial lymphocytes. *Gastroenterology* 115(6):1439–1445.
24. Yajima T, Nishimura H, Saito K, Kuwano H, Yoshikai Y (2004) Overexpression of Interleukin-15 increases susceptibility to lipopolysaccharide-induced liver injury in mice primed with *Mycobacterium bovis* bacillus Calmette-Guérin. *Infect Immun* 72(7):3855–3862.
25. Tani-ichi S, et al. (2013) Interleukin-7 receptor controls development and maturation of late stages of thymocyte subpopulations. *Proc Natl Acad Sci USA* 110(2):612–617.
26. McCaughtry TM, et al. (2012) Conditional deletion of cytokine receptor chains reveals that IL-7 and IL-15 specify CD8 cytotoxic lineage fate in the thymus. *J Exp Med* 209(12):2263–2276.
27. Noda M, et al. (2011) CXCL12-CXCR4 chemokine signaling is essential for NK-cell development in adult mice. *Blood* 117(2):451–458.
28. Estess P, Nandi A, Mohamadzadeh M, Siegelman MH (1999) Interleukin 15 induces endothelial hyaluronan expression in vitro and promotes activated T cell extravasation through a CD44-dependent pathway in vivo. *J Exp Med* 190(1):9–19.
29. Sancho D, Yáñez-Mó M, Tejedor R, Sánchez-Madrid F (1999) Activation of peripheral blood T cells by interaction and migration through endothelium: Role of lymphocyte function antigen-1/intercellular adhesion molecule-1 and interleukin-15. *Blood* 93(3):886–896.
30. Andonegui G, et al. (2003) Endothelium-derived Toll-like receptor-4 is the key molecule in LPS-induced neutrophil sequestration into lungs. *J Clin Invest* 111(7):1011–1020.
31. Kang S, et al. (2009) Toll-like receptor 4 in lymphatic endothelial cells contributes to LPS-induced lymphangiogenesis by chemotactic recruitment of macrophages. *Blood* 113(11):2605–2613.
32. Mortier E, et al. (2009) Macrophage- and dendritic-cell-derived interleukin-15 receptor α supports homeostasis of distinct CD8+ T cell subsets. *Immunity* 31(5):811–822.
33. Moussion C, Girard JP (2011) Dendritic cells control lymphocyte entry to lymph nodes through high endothelial venules. *Nature* 479(7374):542–546.
34. Hara T, et al. (2012) Identification of IL-7-producing cells in primary and secondary lymphoid organs using IL-7-GFP knock-in mice. *J Immunol* 189(4):1577–1584.
35. Nakamura Y, et al. (2010) Isolation and characterization of endosteal niche cell populations that regulate hematopoietic stem cells. *Blood* 116(9):1422–1432.
36. Morikawa S, et al. (2009) Prospective identification, isolation, and systemic transplantation of multipotent mesenchymal stem cells in murine bone marrow. *J Exp Med* 206(11):2483–2496.
37. Kawamoto T (2003) Use of a new adhesive film for the preparation of multi-purpose fresh-frozen sections from hard tissues, whole-animals, insects and plants. *Arch Histol Cytol* 66(2):123–143.
38. Reinhardt RL, Khoruts A, Merica R, Zell T, Jenkins MK (2001) Visualizing the generation of memory CD4 T cells in the whole body. *Nature* 410(6824):101–105.

Supporting Information

Cui et al. 10.1073/pnas.1318281111

SI Materials and Methods

Generation of IL-15–CFP Knock-in Mice. The targeting vector for IL-15–CFP knock-in mice was generated as follows. A diphtheria toxin A cassette was subcloned in the pBluescript KS(+) vector (pBS-DTA). A 1,977-bp genomic DNA fragment of 3′ IL-15 region after the third IL-15 exon was amplified by PCR and subcloned in the pBS-DTA vector (pBS-3′IL15-DTA). The enhanced CFP cassette and neomycin resistance gene cassette flanked by two *loxP* sites (LNL) were amplified by PCR and inserted into the pBS-3′IL15-DTA vector (pBS-CFP-LNL-3′IL15-DTA). A 7,999-bp genomic DNA fragment of the 5′IL-15 region upstream of the initiation codon in the third IL-15 exon was amplified by PCR and subcloned into the pBS-CFP-LNL-3′IL15-DTA vector (pBS-5′IL15-CFP-LNL-3′IL15-DTA; Fig. S1*A*). The linearized targeting vector was introduced into the KY1.1 embryonic stem cell line derived from a C57BL/6J × 129S6/SvEv-Tac mouse embryo (gift from Junji Takeda, Osaka University, Osaka, Japan). Homologous recombinants were screened by PCR and confirmed by Southern blot analysis with a 3′ probe (Fig. S1*B*). Targeted ES clones were microinjected into ICR eight-cell embryos. Chimeric mice were bred with CAG-Cre transgenic mice to delete the neomycin cassette. Resultant mice containing the enhanced CFP cDNA within the endogenous IL-15 locus were backcrossed to C57BL/6 mice for at least six generations.

Multiphoton Tissue Imaging. Intravital imaging of mouse calvaria bone was realized as described previously (1, 2). In brief, the frontoparietal regions of the calvaria of anesthetized mice were exposed and fixed on a customized microscope stage. The bone marrow cavity was observed by using a multiphoton imaging system composed of a multiphoton upright microscope (A1-MP; Nikon) equipped with a 25× water immersion objective (APO,

NA 1.1; Nikon). Sample excitation was provided by a Chameleon Vision II Ti:Sapphire laser (Coherent) tuned at 820 nm, and emitted fluorescence was collected by using a GaAsP multi-detector unit (Nikon). ECFP- and EGFP-expressing cells were detected through a bandpass emission filter at 483/32 nm and 525/50 nm, respectively, and discriminated from second harmonic generation (SHG) signals (representing bone tissue) by a bandpass emission filter at 414/46 nm. Blood vessels were visualized by injecting nonfunctionalized eFluor 650 nanocrystals (detected using a 593/40 nm bandpass filter; eBioscience) i.v. immediately before imaging. Image stacks were collected at 2 μm vertical step size at a depth of 100 to 150 μm below the skull bone surface. Multiphoton imaging of thymus was performed on explanted tissues with the multiphoton inverted microscope as described for calvaria. Raw imaging data were processed with NIS-Elements software (Nikon) and analyzed using Imaris software (Bitplane) with a Gaussian filter for noise reduction.

Antibodies. The following fluorescent dye- or biotin-conjugated antibodies were used: anti-GFP, Alexa Fluor 488–anti-GFP, Alexa Fluor 546–anti-rabbit IgG, and streptavidin–Alexa Fluor 488 (BioLegend); allophycocyanin (APC)–Cy7–anti-CD45, APC–Cy7–anti-CD11c, APC–Cy7–anti-CD11b, Alexa Fluor 647–anti-Ly51, PE–anti-EpCAM, Pacific Blue–anti-MHC-II, APC–anti-CD31, Brilliant Violet 421–anti-CD31, APC–anti-CD140b (PDGFRβ), PE–Cy7–anti-Sca-1, biotin–anti-Podoplanin (gp38), and APC–anti-CD3 (Invitrogen); eFluor 450–anti-CD8, APC–Cy7–anti-B220, PE–anti-CD11c, FITC–anti-F4/80, biotin–anti-rat IgG, and PE- or APC-streptavidin (eBioscience); and FITC–anti-CD31, APC–anti-CD11c, and APC–anti-CD11b (BD Pharmingen). Biotin–anti–VCAM-1 was a gift of Tatsuo Kina (Kyoto University, Kyoto, Japan).

1. Ishii M, et al. (2009) Sphingosine-1-phosphate mobilizes osteoclast precursors and regulates bone homeostasis. *Nature* 458(7237):524–528.

2. Ishii M, Kikuta J, Shimazu Y, Meier-Schellersheim M, Germain RN (2010) Chemorepulsion by blood S1P regulates osteoclast precursor mobilization and bone remodeling in vivo. *J Exp Med* 207(13):2793–2798.
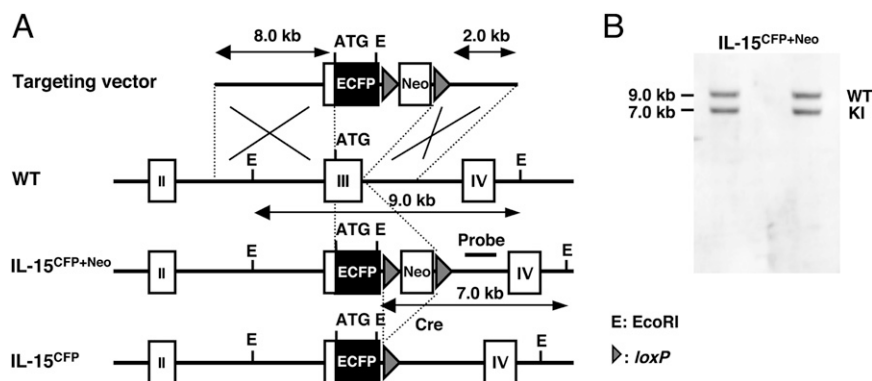
Fig. S1. Generation of IL-15–CFP knock-in mice. (*A*) Targeting strategy for the IL-15–CFP knock-in allele. Boxes indicate exons and cDNAs. ATG indicates the translation initiation codon. Triangles indicate loxP sequences. Horizontal bars indicate the probe. The neomycin resistance gene cassette was excised by Cre recombination. (*B*) Genomic DNA from targeted ES cells was digested with EcoRI and analyzed by Southern blot analysis with the 3′ probe shown in *A*. WT and targeted allele (KI) samples gave rise to 9.3- and 7.0-kb EcoRI fragments, respectively.
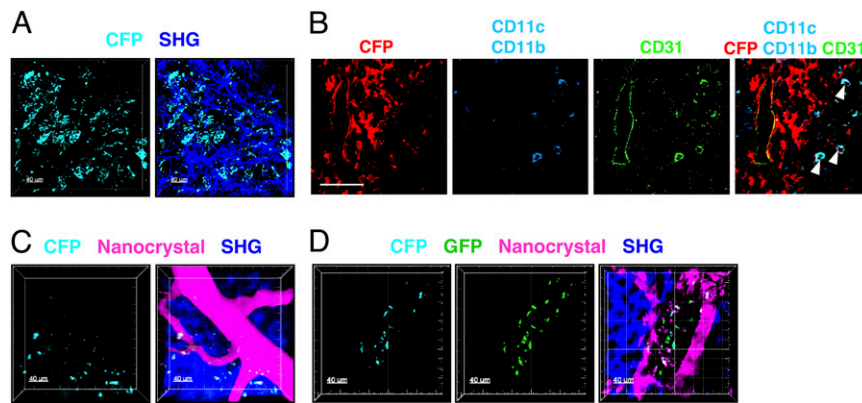
Fig. S2. IL-15 expression in thymus and bone marrow. (*A*) Multiphoton fluorescence in vivo images of the IL-15–CFP knock-in thymus with CFP-labeled cells (turquoise; *Left*) and collagen fibers visualized by SHG signals (dark blue; *Right*). (*B*) Immunohistochemical analysis to detect IL-15 expression in dendritic cells (DCs) and macrophages of IL-15–CFP knock-in thymus (arrowheads). DCs and macrophages were stained with anti-CD11c (blue) and anti-CD11b (blue) antibodies. (Scale bar, 50 μm.) (*C*) Multiphoton fluorescence in vivo images of the bone marrow with CFP-labeled cells (turquoise; *Left*) and the bone matrix visualized by SHG signals (dark blue; *Right*) and blood vessels stained with nanocrystals (purple; *Right*). Data represent two independent experiments with similar results. (Scale bar, 40 μm.) (*D*) Multiphoton fluorescence in vivo images of the IL-15–CFP/IL-7–GFP double knock-in bone marrow with CFP-labeled cells (turquoise; *Left*), GFP-labeled cells (green; *Middle*), and the bone matrix visualized by SHG signals (dark blue; *Right*) and blood vessels stained with nanocrystals (purple; *Right*). Data represent two independent experiments with similar results. (Scale bar, 40 μm.)
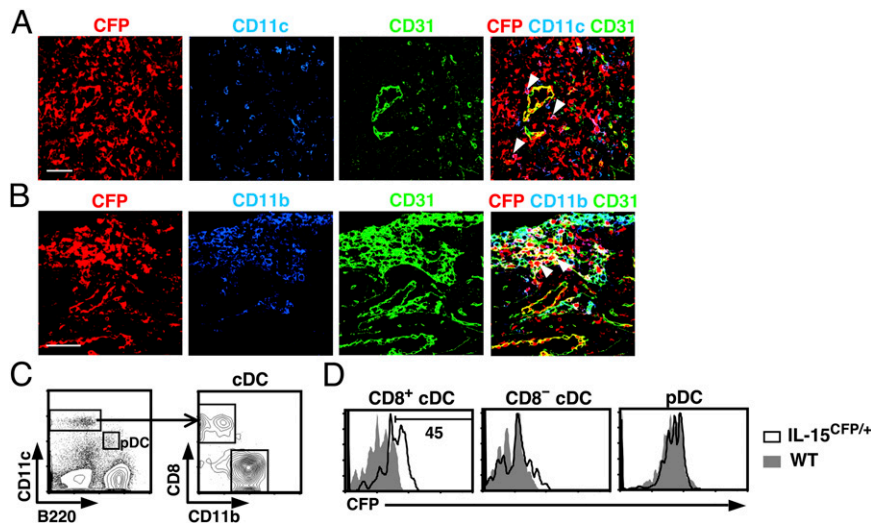
Fig. S3. IL-15 expression in hematopoietic subsets of lymph nodes and spleen. IL-15 expression in lymph nodes and spleen of 6- to 10-wk-old IL-15–CFP knock-in mice (IL-15$^{CFP/+}$) and control WT littermates. CFP signals were detected with anti-GFP antibody. (*A*) Immunohistochemical analysis of DCs in lymph nodes (arrowheads). DCs were stained with anti-CD11c (blue) antibody. (Scale bar, 50 μm.) (*B*) Immunohistochemical analysis of macrophages in lymph nodes (arrowheads). Macrophages were stained with anti-CD11b (blue) antibody. Triple stained (red, green, and blue overlap) cells appear white. (Scale bar, 50 μm.) (*C*) Separation of DC subsets. (*D*) IL-15 expression in CD8$^+$ and CD8$^-$ conventional DCs (cDCs; CD11c$^+$B220$^-$) and plasmacytoid DCs (pDCs; CD11c$^+$B220$^+$). Data represent three independent experiments with similar results.
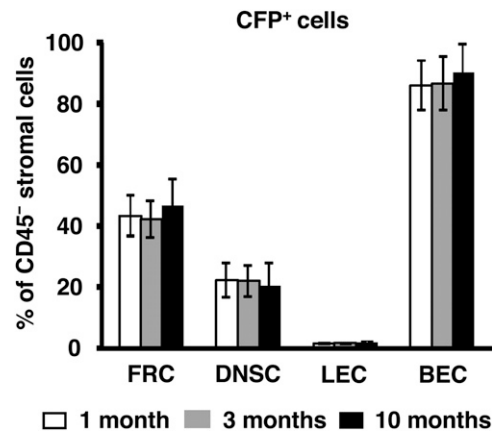
Fig. S4. IL-15 expression in lymph node stromal cells during aging. Single cells were isolated from axillary, cervical, and inguinal lymph nodes of 1-, 3- and 10-mo-old IL-15–CFP knock-in mice (IL-15$^{CFP/+}$) and control WT littermates. Percentages of CFP^{high} stromal cells are shown. Values are the mean ± SEM of three independent experiments.
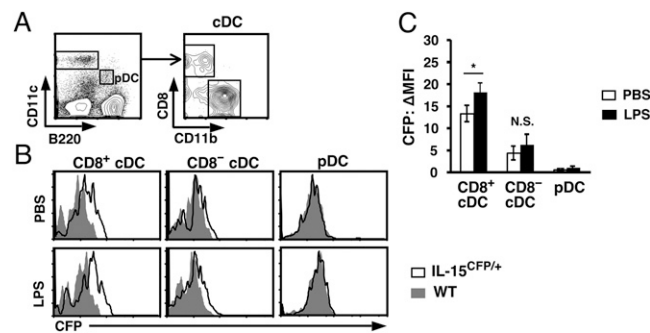

Fig. S5. IL-15 induction in DC subsets after LPS administration. (*A*) Separation of DC subsets. (*B*) IL-15 expression in DC subsets from 6- and 10-wk-old IL-15–CFP knock-in mice and control WT littermates 3 d after injection of PBS solution (control; *Upper*) or LPS (*Lower*). (*C*) The difference in mean fluorescence intensity (ΔMFI) values of CFP between LPS-stimulated and nonstimulated mice as shown in *B*. Values are the mean ± SEM of three independent experiments.
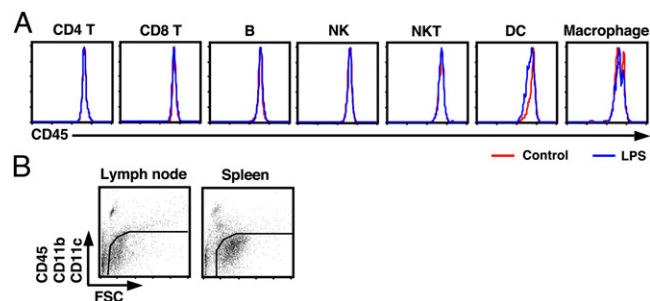

Fig. S6. Elimination of hematopoietic cells in flow cytometric analysis. (*A*) CD45 expression in hematopoietic subsets. Flow cytometric analysis of spleen cells 3 d after injection of PBS solution or LPS. (*B*) CD45$^-$CD11b$^-$CD11c$^-$ gated stromal cell fractions in lymph nodes and spleen. Data represent at least three independent experiments with similar results.
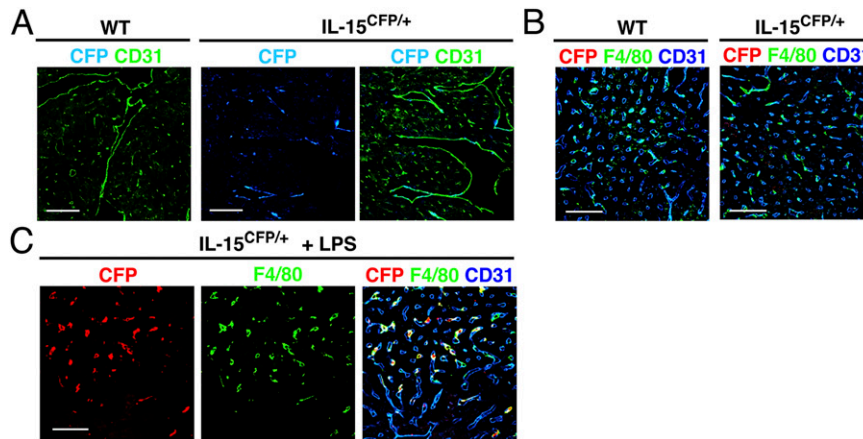
Fig. S7. IL-15 expression in heart and liver. IL-15 expression in heart and liver of 6- to 12-wk-old IL-15–CFP knock-in mice (IL-15$^{CFP/+}$) and control WT littermates. CFP signals were detected with anti-GFP antibody. (*A*) Immunohistochemical analysis of heart. Endothelial cells were stained with anti-CD31 antibody. CFP$^+$ CD31$^+$ cells (blue and green overlap) appear turquoise. (*B*) Immunohistochemical analysis of liver. Macrophages and endothelial cells were stained with anti-F4/80 and anti-CD31 antibodies, respectively. (*C*) Immunohistochemical analysis of liver 3 d after LPS injection. CFP$^+$ macrophages (red and green overlap) appear yellow. Data represent two independent experiments with similar results. (Scale bar, 50 μm.)

Table S1. IL-15- and IL-7–expressing stromal cells in primary and secondary lymphoid organs

Organ	IL-15–expressing cell	IL-7–expressing cell
Thymus	MHC-II^{high} mTEC, BEC, Pericyte*	mTEC, cTEC
Bone marrow	VCAM-1$^+$PDGFRβ^{high}CD31$^-$Sca-1$^-$cell (CAR cell)*	VCAM-1$^+$CD31$^-$ and VCAM-1$^+$CD31$^+$ cell*
	VCAM-1$^+$PDGFRβ^{low}CD31$^-$Sca-1$^-$ cell*	PDGFRα$^+$Sca-1$^-$ and PDGFRα$^+$Sca-1$^+$ cell*
Lymph node	BEC, FRC*, DNSC*	LEC, FRC*
Spleen	VCAM-1$^+$ stromal cell*	FRC*
Intestine	BEC, IEC*	LEC, IEC*

*Some cells are positive. BEC, blood endothelial cells; CAR, CXCL12-abundant reticular; cTEC, cortical thymic epithelial cell; DNSC, double-negative stromal cells; FRC, fibroblastic reticular cell; IEC, intestinal epithelial cell; LEC, lymphatic endothelial cell; mTEC, medullary thymic epithelial cell.